Unimolecular dissociation rates of the chlorobenzene cation prepared by multiphoton ionization

J. L. Durant, D. M. Rider,[a] S. L. Anderson,[b] F. D. Proch,[c] and R. N. Zare
Department of Chemistry, Stanford University, Stanford, California 94305

(Received 30 September 1983; accepted 17 November 1983)

We have studied the unimolecular reaction $C_6H_5Cl^+ \rightarrow C_6H_5^+ + Cl$ as a function of internal energy by using multiphoton ionization (MPI) on a supersonically cooled jet of chlorobenzene to prepare the excited parent ion. Specific rate constants $k(E)$ were obtained from an analysis of the distorted $C_6H_5^+$ peak shape in a time-of-flight (TOF) mass spectrometer. Decomposition in the wavelength region 265–270 nm is shown to proceed by two-photon ionization followed by one-photon absorption. The internal energy of the excited parent ion is characterized in a separate experiment which measures the photoelectron kinetic energy distribution, obtained over the same wavelength range. The specific rate constants found in this study compare well with previous literature values, thus validating this MPI TOF technique for the determination of ion decomposition rates.

I. INTRODUCTION

A great variety of techniques have been used to measure rates of ionic unimolecular reactions.[1] Most suffer, however, from a gross lack of knowledge of the distribution of internal energy with which the activated ion is formed. One technique, photoion-photoelectron coincidence[2–6] (PIPECO), largely overcomes this problem. In a typical PIPECO experiment the molecular sample is ionized by monochromatic vacuum ultraviolet (VUV) radiation, usually produced by a discharge continuum source in conjunction with a monochromator. The arrival of daughter ions is detected in delayed coincidence with zero kinetic energy electrons to generate a decay curve for the parent. With a knowledge of the photon energy and the ionization potential (I.P.) of the parent molecule the PIPECO data yield the rate of daughter ion appearance averaged over a narrow distribution of parent internal energies. This averaging process depends on the thermal energy spread in the parent molecule convoluted with the variation of the absorption cross section over this Boltzmann distribution.

Recent work has also characterized the energy distributions obtained in field ionization mass spectroscopy,[7,8] allowing field ionization kinetics (FIK) to be applied to quantitative determination of $k(E)$ curves.[9] In this technique metastable ions formed in a high temperature field ionization source are detected, and the integral decomposition rate for the almost thermal parent ions, and ultimately the $k(E)$ curve, are extracted.

Another technique that shows promise as a source of energy-selected ions is multiphoton ionization (MPI). Previously, we have reported the application of MPI time-of-flight (TOF) mass spectrometry to the measurement of the dissociation rates of aniline[10] in which a "metastable" parent ion decays to a daughter ion during acceleration, causing the appearance of an asymmetric time-of-arrival distribution of the daughter ion. The results demonstrated that (1) dissociation rates of ions prepared by MPI can be measured and (2) the internal energy of the reactant ion depends on the excitation wavelength. A subsequent PIPECO study of aniline[11] corroborated the MPI data suggesting that energy-selected dissociation rates can be measured with this MPI TOF technique. A study has also been made on the unimolecular decomposition of MPI-generated ions in the field-free region of a reflectron-type TOF mass spectrometer in which the decay of $C_6H_6^+$ metastables was directly observed.[12]

The experimental apparatus used in the study of the unimolecular decomposition of the aniline cation did not allow a direct measurement of the reactant ion's internal energy. We have extended our capabilities by the addition of a supersonic molecular beam, giving us neutral precursors with a narrow energy distribution, and by construction of a photoelectron spectrometer, allowing us to determine the distribution of ionic states initially populated by MPI.[13–18] By combining this information with the data from the MPI TOF technique, the energy-selected rate constants for dissociation of ions are found.

Chlorobenzene was chosen to serve as a test case. We studied the rate of the reaction

$$C_6H_5Cl^+ \rightarrow C_6H_5^+ + Cl$$

as a function of reactant ion internal energy. The $k(E)$ values of this reaction have been measured previously in several independent experiments.[19–21] The results are overall in good but not perfect agreement. Further, the energetics of the chlorobenzene system are fairly well established so that the existing body of data provides a sound basis for the interpretation of the MPI results.

The success of MPI as a method for preparing reactant ions is based on the degree to which ions can be produced with a narrow and known distribution of internal energies. The fulfillment of this requirement depends on the precise mechanism of ionization by multiphoton adsorption. In par-

[a] Present address: Jet Propulsion Laboratory, California Institute of Technology, Pasadena, California 91103.
[b] Department of Chemistry, State University of New York, Stony Brook, New York 11794.
[c] MPI für Quantenoptik, D 8046 Garching, Federal Republic of Germany.

 0021-9606/84/051817-09$02.10

ticular, the number of photons absorbed before ionization occurs energetically constrains the number of ion states and the distribution of vibrational levels of each state that can be initially populated by MPI. In addition to this energetic constraint, vibronic selection rules and the Franck–Condon principle control the final ion state distribution.[13] In this way, the vibrational levels of any intermediate state influence the vibrational energy distribution of the ion. In this paper we carefully examine the MPI mechanism for chlorobenzene.

The dissociation rate of chlorobenzene ions ($C_6H_5Cl^+$) to form the phenyl ion ($C_6H_5^+$) is determined from the asymmetrically broadened phenyl ion TOF peak shape. We report the wavelength dependence of the dissociation rate, derive the specific rate constants for energy-selected ions, and compare these to the previously measured rates.[19–21]

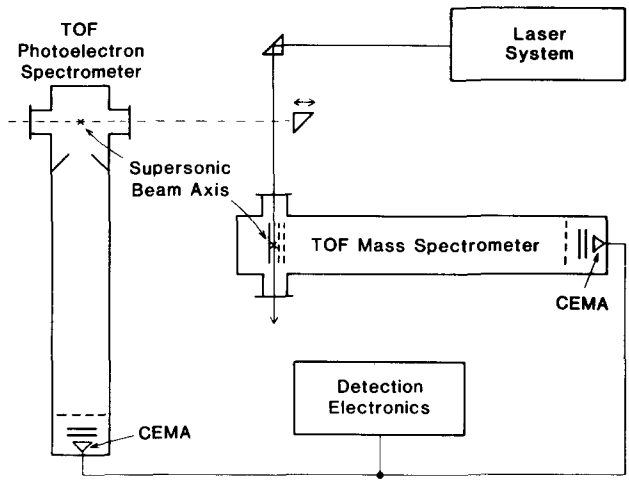

FIG. 1. Experimental setup. A TOF mass spectrometer and a TOF photoelectron spectrometer use the same laser system and common detection electronics.

II. EXPERIMENTAL

Separate instruments are used to record mass spectra and photoelectron spectra; however, both use the same laser and detection electronics. A schematic of the experimental setup is shown in Fig. 1.

The light source is a Nd:YAG pumped dye laser (Quanta-Ray DCR-lA and PDL) whose output is frequency doubled with an angle-tuned KD*P crystal. The phase matching angle is maintained with a home-built autotracker that incorporates the electronic design of Bjorklund and Storz.[22] The doubling crystal output is dispersed and the UV beam is directed into either the TOF mass spectrometer or the TOF photoelectron spectrometer. Coumarin 500 (Exciton Chemical Co.) was used to cover the wavelength region between 265 and 270 nm.

For the measurement of dissociation rates, a 35 cm focal length lens was used to focus the laser, with typical power densities of ~ 15 MW/cm^2. For photoelectron spectra, the laser beam is focused with a 150 mm focal length cylindrical lens. Typical photoelectron spectra are recorded at a laser power density of about 5 MW/cm^2. The angle between the laser polarization and the detection axis is 0°. The angular distribution of the photoelectrons is found to be weakly peaked along the laser polarization vector ($I_{\parallel}/I_{\perp} \simeq 1.5$) and is independent of final ion vibrational state.

The TOF mass spectrometer is described in Ref. 10. However, the dimensions of the ion source (Fig. 2) have been modified to increase ion residence times in region I. Also, a pulsed nozzle (Quanta-Ray PSV-1) supersonic beam has been added. The pulsed nozzle is differentially pumped by a water-baffled 6 in. diam diffusion pump. A skimmer with a 1 mm diam orifice is located 1 cm downstream from the 0.5 mm diam nozzle. The skimmer-to-interaction region distance is 20 cm. The beam composition is typically 0.06% chlorobenzene seeded in helium and is used at a stagnation pressure of 1.3 atm. The time averaged pressure is 6×10^{-7} Torr in the mass spectrometer chamber when the nozzle is operating. Undiluted room temperature samples are admitted via a leak valve. In this case, the sample pressure is maintained at 2×10^{-6} Torr.

Mass spectra are recorded with a programmable transient digitizer (Tektronix 7912 AD) interfaced to a microcomputer system (Cromemco Z2). Typically, data from 1000–5000 laser shots are averaged with the digitizer-computer system. Wavelength spectra of selected ion peaks (ion yield spectra) are acquired using a boxcar integrator (PARC Model 162 with 164 and/or 165 plug ins) and displayed on a strip chart recorder.

The photoelectron spectrometer is discussed in Ref. 13. Briefly, it consists of a magnetically shielded, 50 cm long, field-free flight tube that is evacuated with a 110 l/s turbomolecular pump (Balzers TPU 110). A conical baffle with a 2 cm diam hole is placed in the flight tube. The photoelectrons are detected with a channel electron multiplier array (CEMA) (Galileo FTD 2003). Arrival times are recorded using the programmable transient digitizer.

Chlorobenzene (Aldrich Chemical Co.; 99.5% pure) was degassed by several freeze-pump-thaw cycles before use.

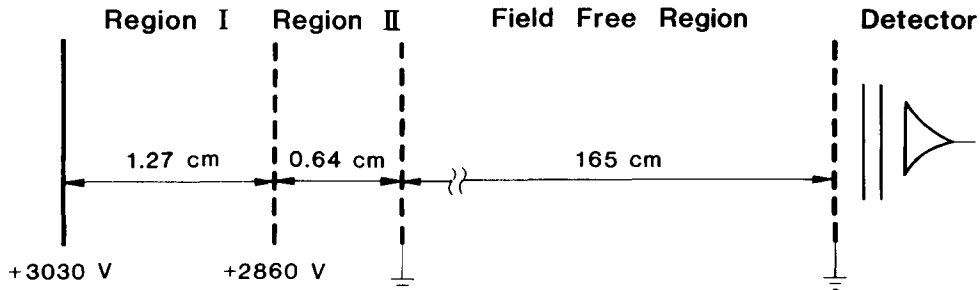

FIG. 2. TOF mass spectrometer dimensions and potentials.

III. RESULTS AND DISCUSSION

A. Ionization and excitation pathways

Before we can study the formation of phenyl ions from chlorobenzene, we need to establish that the phenyl ion does, in fact, arise from chlorobenzene; further, we must characterize the ionization process.

If we examine the pertinent energy level diagram shown in Fig. 3, we note that by pumping in the UV we should be able to photoionize the chlorobenzene in a two-photon process, utilizing the $\tilde{A}\ ^1B_2$ state of the neutral for resonant enhancement. Absorption of a third photon should produce a chlorobenzene cation with sufficient energy to fragment.

The parent ion yield spectrum (Fig. 4) indeed implicates the $\tilde{A}\ ^1B_2$ state in the ionization process. The room temperature spectrum [Fig. 4(a)] agrees well with the one-photon absorption spectrum for the $\tilde{A}$ state reported by Jain and Bist.[23] The relative band intensities are somewhat different, but this discrepancy can be entirely attributed to the intensity variation of the dye laser with wavelength. The spectrum is sufficiently congested with hot bands and rotational structure that given the $\sim 0.5\ cm^{-1}$ bandwidth of the laser, ionization appears essentially continuous.

In contrast, the jet-cooled spectrum [Fig. 4(b)] is quite discrete. We estimate the rotational temperature to be less than 50 K. All the bands in the cold spectrum can be assigned to fundamental and combination hot bands observed in the room temperature spectrum. Vibrational cooling is evident, though difficult to quantify.

When we examine the phenyl ion yield spectrum, we find it to be identical, except for relative intensity variations, with the parent ion yield spectrum. This establishes that the metastable peak arises ultimately from neutral chlorobenzene.

The MPI TOF mass spectrum of chlorobenzene is shown in Fig. 5. The laser wavelength is 266 nm at a power density of $\sim 2\ MW/cm^2$. The parent ion ($m/e = 112$–115) and the phenyl ion ($m/e = 77$–78) dominate the mass spectrum at and below this power density. However, the extent of fragmentation of the chlorobenzene cation depends strongly on the laser power density in agreement with MPI studies on several other organic compounds.[24–26] Over 25 different fragment ions are detected at a power density of $\sim 100\ MW/cm^2$.

The phenyl ion peak (Fig. 6) is found to be broadened toward high mass (long time). The asymmetry results from the dissociation of more massive ions during acceleration in the ion source of the TOF mass spectrometer. The only charged precursor possible is the chlorobenzene cation. The phenyl ion peak shape depends strongly on the dissociation rate and provides the basis of our absolute rate measurements.

A competing pathway for the delayed production of phenyl ions may be the ion-pair formation of $C_6H_5^+$ and Cl^-. Thermochemically, this process first becomes possible following the absorption of three UV photons. To check for this possibility, the fields were reversed in the TOF mass spectrometer, so as to generate a negative ion mass spectrum. Under the conditions used in the positive ion studies, the negative ion signals were orders of magnitude smaller. We can thus neglect ion-pair formation in our data analysis.

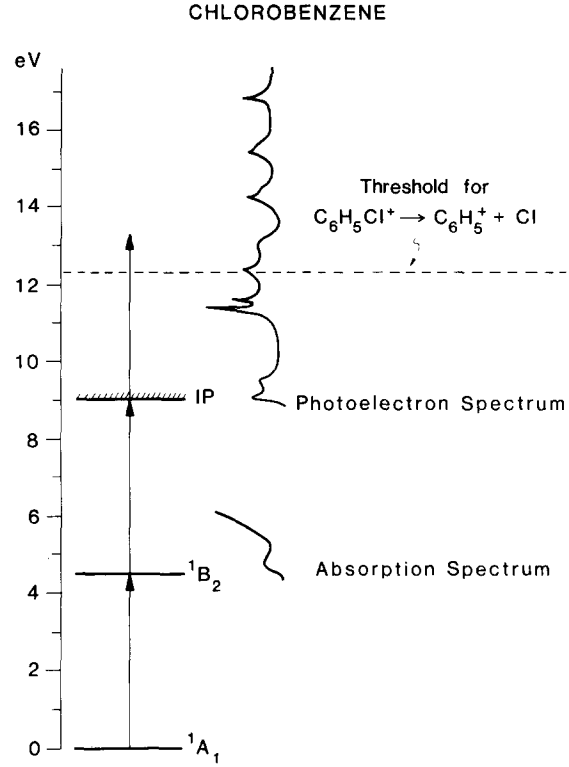

FIG. 3. Chlorobenzene energy level diagram showing onset of absorption and photoionization. The photoelectron spectrum is taken from Ref. 25.

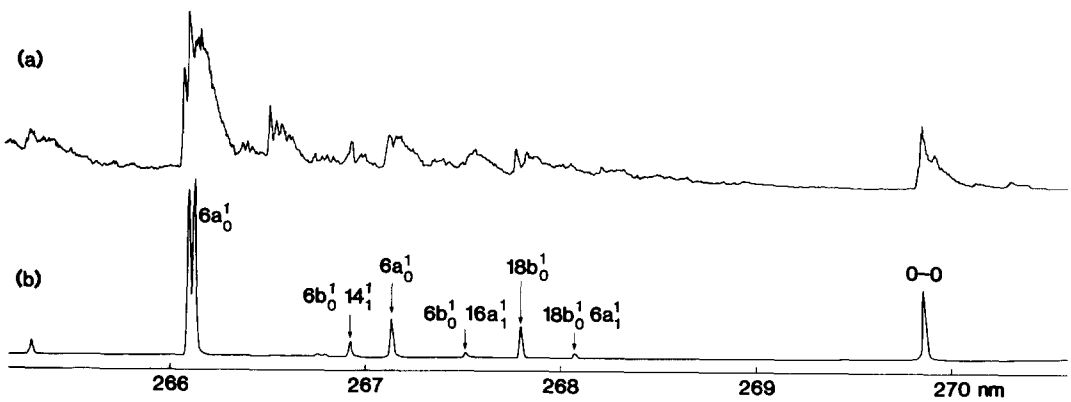

FIG. 4. Parent ion yield spectra of chlorobenzene: (a) room temperature; and (b) jet cooled.

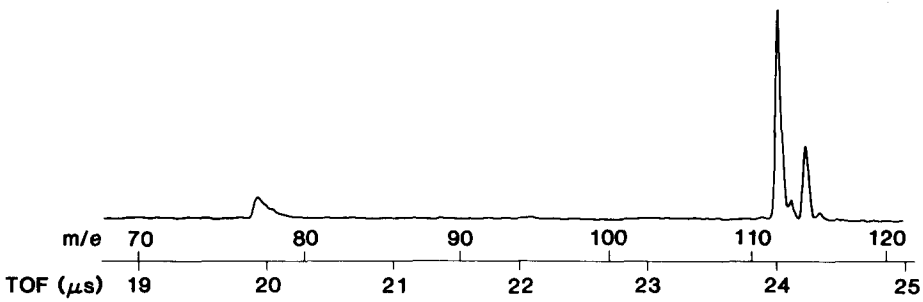

FIG. 5. MPI TOF mass spectrum of room temperature chlorobenzene at 266 nm. The cluster at $m/e = 112$–115 shows the parent ion with its ^{37}Cl and ^{13}C isotopes. The asymmetric mass peak at $m/e = 77$ is the daughter phenyl ion.

Prompt phenyl cation formation is possible by

$$C_6H_5Cl + h\nu \rightarrow C_6H_5Cl^* \rightarrow C_6H_5 + Cl,$$

$$C_6H_5 + 2h\nu \rightarrow C_6H_5^+ + e^-.$$

However, this pathway will not give rise to a metastable peak; also difficulties in ionizing highly excited aromatics,[27] presumably due to Franck–Condon considerations, argue strongly against this possibility.

Having established the source of the phenyl ion as being the decomposition of the chlorobenzene cation, we are then faced with the task of determining how the chlorobenzene ionizes. MPI photoelectron spectra were recorded at various wavelengths in the 265–270 nm range. A representative spectrum is shown in Fig. 7. In no case were photoelectrons observed with kinetic energies greater than that allowed by conservation of energy for two-photon ionization of chlorobenzene.[13] We can conclude that ionization takes place after the absorption of two UV photons by the neutral chlorobenzene. This finding is in agreement with the results of several other studies on benzene and toluene which suggest that ionization often occurs by the absorption of the minimum number of photons required to exceed the lowest I.P.[13–15,25] The width of the photoelectron energy distribution varies but never exceeds 150 meV. The spectra do have resolved vibrational structure and their assignment is discussed elsewhere.[13] All features in the photoelectron spectra could be assigned to ionization of chlorobenzene. This supports the conclusion that the phenyl ion arises predominantly from dissociation of the chlorobenzene cation.

The chlorobenzene ions formed at the two-photon level are constrained to have less than 250 meV of excess energy; they therefore lack sufficient energy to dissociate. Hence, the absorption of three or more photons is required to produce the phenyl daughter ion. The chlorobenzene cation has a number of excited electronic states at the three-photon level, as shown by its HeI photoelectron spectrum[28] (see Fig. 3). While it is likely that initial excitation of the cation occurs to one of these states, it appears that the molecule rapidly undergoes some nonradiative process. Evidence for this is the lack of observed fluorescence from the chlorobenzene cation.[29] If we assume that internal conversion occurs to the ground state, then classical RRK calculations suggest that the rate for chlorine atom elimination at the three-photon level is on the order of $10^5\ s^{-1}$ while at the four-photon level

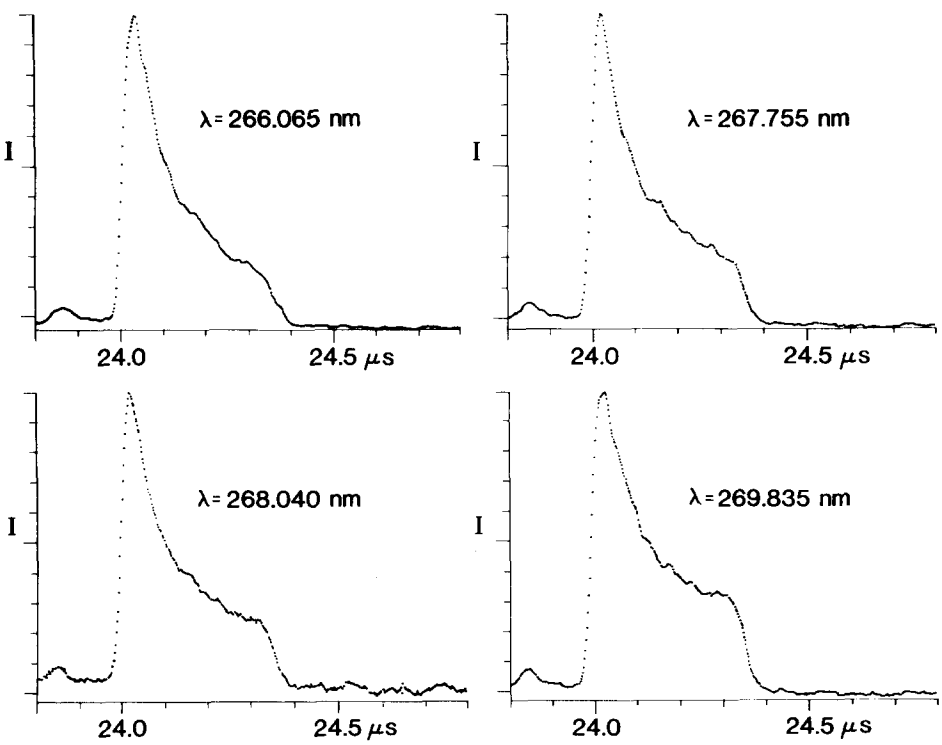

FIG. 6. Phenyl ion mass peak shape as a function of excitation wavelength.

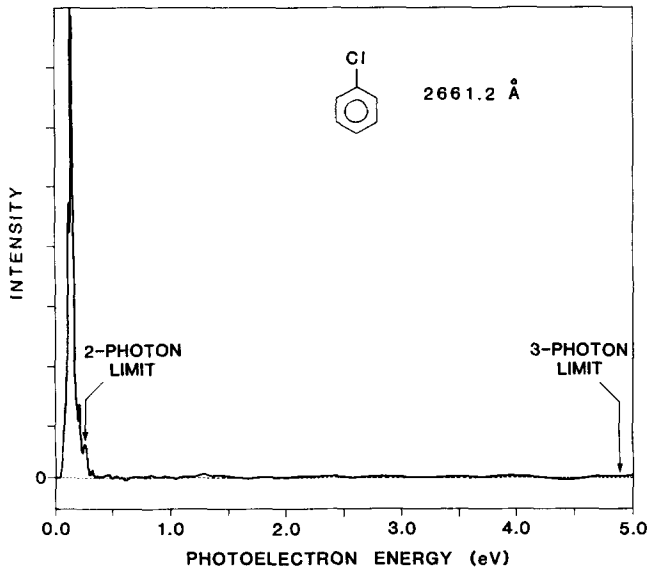

FIG. 7. TOF photoelectron spectrum of chlorobenzene.

it is orders of magnitude larger. Because we can observe significant peak broadening only for rates between 10^5–$10^7\ s^{-1}$, we conclude we are measuring rates for the decomposition of chlorobenzene cations that have absorbed one UV photon, i.e., an overall three-photon process. Some additional support for one-photon dissociation of chlorobenzene cations is provided by Dunbar, Teng, and Fu,[30] who have demonstrated through an ion cyclotron resonance experiment that the cation is dissociated by light in the 4–5 eV range.

B. Dissociation rates

The qualitative dissociation rate dependence of the metastable mass peak can best be understood with reference to Fig. 8. Stable ions are accelerated through regions I and II and arrive at the detector at mass dependent times, in accord with the elementary laws of electrostatics. However, if the ion decomposes as it is accelerated, it will be detected at a time intermediate between the flight times of the parent and daughter ions. In particular, Fig. 8 shows the TOF for a chlorobenzene ion fragmenting to form a phenyl ion. One should note that the first microsecond of the parent ion lifetime maps onto 350 ns in the measured time of flight. The next 500 ns, however, is stretched into almost 4.5 μs in the measured TOF. This leads to a marked attenuation of the signal from ions dissociating in region II, so much so that experimentally it is observed only as a somewhat noisy base line. In the case of a first order decay one should expect the metastable mass peak to be roughly exponentially decreasing, with a sharp drop at about 350 ns, corresponding to the parent ion residence time in region I.

A number of other factors cause broadening in the detected peak width. They include the spread in initial positions caused by the finite laser spot size and the spread in initial velocities caused by thermal motion of the parent molecule. Additionally, inhomogenities in the fields, detector and electronic response speeds, and other sources contribute to the observed spread. All these factors, taken together, constitute what we call the instrument response function Φ. This function is experimentally obtained by measuring the line shape of the parent mass peak $^{12}C_6H_5\,^{35}Cl^+$, which is the response of the mass spectrometer to a delta function pulse of ions. This instrumental broadening was removed by use of a Fourier transform based deconvolution algorithm. (See the Appendix.) After the deconvolution had been performed, it was a straightforward task to subtract the isotopic contributions to the peak shape arising from ^{13}C and ^{37}Cl, and convert the measured time-of-flight distribution $H(T)$ to a reaction time distribution $h(t_r)$. Typical input peak shapes and resulting decay curves are shown in Fig. 9.

In the above, we have neglected effects of kinetic energy

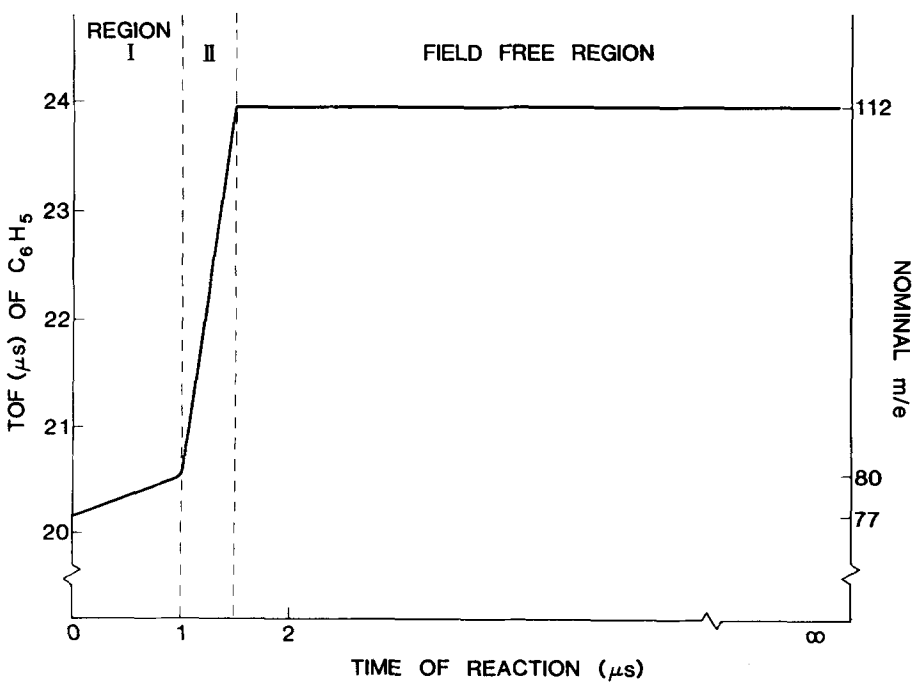

FIG. 8. Relation between arrival time of the daughter ion $C_6H_5^+$ and the time of reaction: $C_6H_5Cl^+ \rightarrow C_6H_5^+ + Cl$.

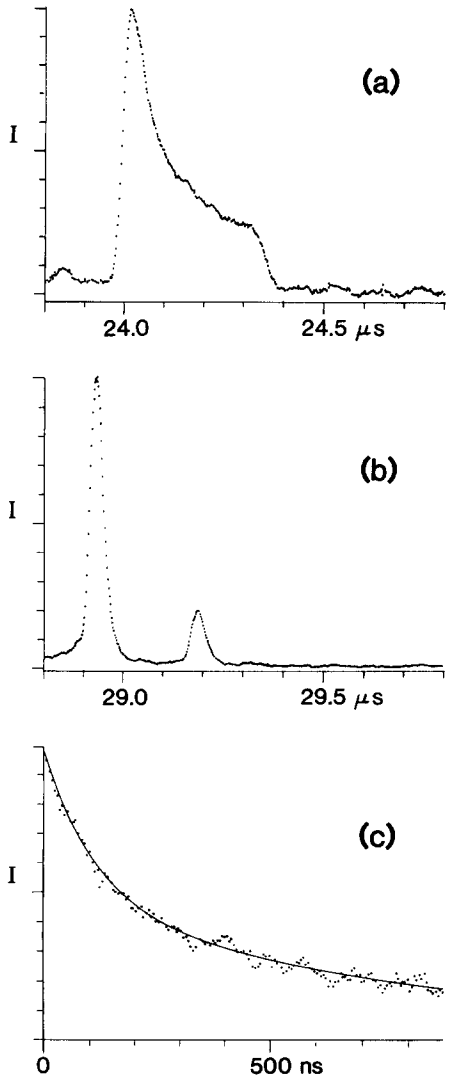

FIG. 9. Typical (a) metastable peak shape, (b) parent mass peak, and (c) resultant intensity vs reaction time plot.

release during fragmentation because the fragmentation occurs in a high field region where the ions are acquiring energies much in excess of that from kinetic energy release. We have also assumed that we could separate the problem into a deconvolution of the initial position and velocity distributions, which are implicitly included in the instrumental response function Φ, followed by the mapping of $H(T)$ onto $h(t_r)$. The assumption of separability was tested by use of Monte Carlo calculations. Let $f(z_0)$, $g(v_0)$, and $h(t_r)$ be the distributions of the initial position, velocity, and reaction time. A random triplet (z_0,v_0,t_r) is selected from the distributions $f(z_0)$, $g(v_0)$, and $h(t_r)$ and followed through a computer-generated model of the mass spectrometer until it arrives at time T at the detector. With a suitably large sample of triplets, typically 5000–10 000, a noisier-than-experimental metastable peak shape emerges. We find that an analysis of this computer-generated peak shape by the same method used to treat the experimental data gives the same rate constant as was used to generate the Monte Carlo mass peak shape. This result encourages us to believe that our data analysis scheme is accurate.

Analysis of the experimental data revealed that all the decays consisted of two components; a fast component which was essentially Fourier transform bandwidth limited, and a slower, exponential decay. Studies of the peak shape as a function of laser power density form 0.35 to 25 MW/cm^2 reveal that the rate constant for the slow decay is power independent, while the relative intensities of the fast and slow components vary noticably, with the fast component becoming less pronounced as the laser power density is decreased. This indicates that the fast and slow components of the decomposition arise from different ensembles of chlorobenzene cations. We ascribe the slow component, which has a noticeable energy dependence, to the decomposition of chlorobenzene cations from their ground electronic state after the (overall) absorption of three UV photons. The fast component can be tentatively ascribed to chemistry at the (overall) four-photon level, though the almost total lack of information about the chlorobenzene cation makes this little more than speculation.

The energies of the parent dissociating ion were calculated from the three-photon energy by adding the thermal energy of the neutral and substracting the sum of the ionization potential of chlorobenzene (I.P. $= 9.066 \pm 0.005$ eV)[31] and an average photoelectron energy. The photoelectron energies were obtained from photoelectron spectra taken at 269.8, 268.04, 267.76, 266.89, 267.10, and 266.10 nm under beam conditions.[13]

The photoelectron spectra allow us unequivocally to bound the energy of the dissociating chlorobenzene cation, though the detailed population at the three-photon level is obscured by the lack of knowledge of the absorption cross section in the ion. However, we have clear upper and lower bounds on the permissible energies, which is not the case when thermal samples are used.

Figure 10 presents the specific rate constants $k(E)$ plotted against the energy above the ground state of the neutral. The error bars are $\pm 1\sigma$ in rate, and rigorous upper and lower bounds on the energy.

Also shown in Fig. 10 are the experimental data of Baer *et al.*,[19] Rosenstock, Stockbauer and Parr,[20] and Pratt and Chupka.[21] Baer *et al.*[19] used the PIPECO technique to measure the specific rate constants for the chlorobenzene cation. Subsequently, in restudying the decomposition of bromobenzene cation, Baer and Kury[32] have included corrections for the effect of thermal energy in the parent molecule for their one-photon process. We approximate these corrections in plotting the data of Baer *et al.*[19] on the chlorobenzene cation decomposition by simply shifting the energy scale by an amount equal to the average thermal energy of the neutral parent (112 meV).

Rosenstock, Stockbauer, and Parr[20] also used the PIPECO technique to study the decomposition of the chlorobenzene cation. Rather than fit the coincidence time-of-flight spectra as done by Baer *et al.*,[19] they calculate breakdown curves, i.e., the ratio of parent to total ions as a function of photon energy. These breakdown curves are then fit by an RRKM model yielding a $k(E)$ curve, as shown in Fig. 10.

Pratt and Chupka[21] have also estimated the specific

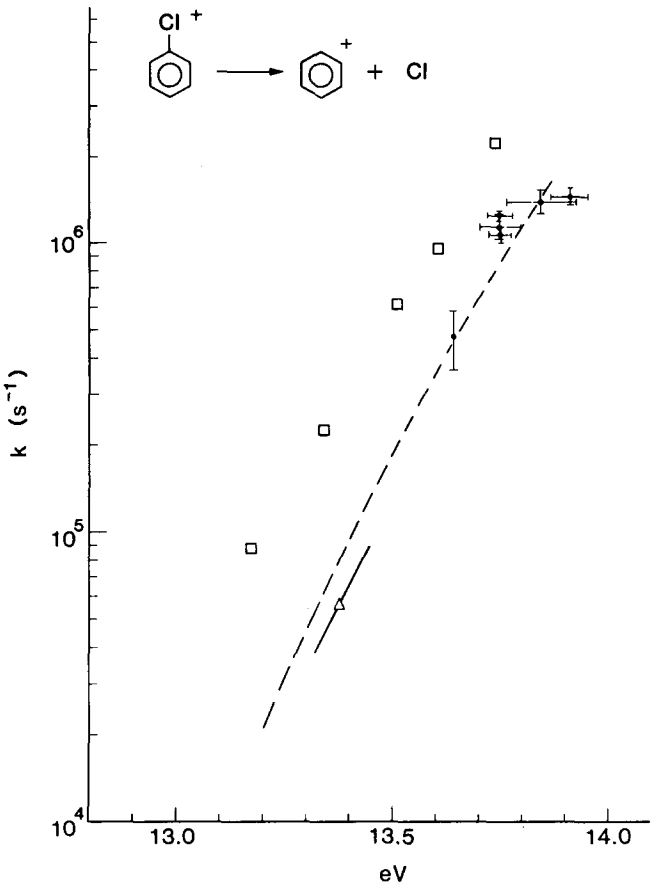

FIG. 10. Specific rate constant as a function of total excitation energy: MPI data (solid circles), PIPECO data of Baer *et al.* (Ref. 16) shifted by 112 meV to account for the average thermal energy in the parent (open squares), RRKM $k(E)$ curve of Rosenstock, Stockbauer, and Parr (Ref. 17) (dashed line), and data of Pratt and Chupka (Ref. 18) (open triangle and line). The vertical error bars on the MPI data line are one standard deviation; the horizontal bars represent rigorous upper and lower bounds on the parent ion internal energy. The point at 13.64 eV arises from excitation of the vibrationless level of the ground state parent ion.

rate constant $k(E)$, based on the intensity of the metastable peak in a magnetic deflection photoionization mass spectrometer. Because of the indirectness of the method, they were only able to extract the rate at maximum metastable ion intensity and the slope of the $k(E)$ curve at that point. Considering the methodology, the agreement is quite good.

Thus, when the thermal energy of the neutral parent is taken into account, all previous determinations of $k(E)$ for the process $C_6H_5Cl^+ \rightarrow C_6H_5^+ + Cl$ are in substantial agreement with the present work. This agreement establishes the capability of the MPI TOF method for determining the unimolecular decay rates of ions.

We have demonstrated that MPI TOF mass spectrometry can be a powerful tool for the measurement of specific rate constants in ion unimolecular decompositions. As presently constituted, we can measure rates from 5×10^5 to $1\times10^7\,s^{-1}$, with good control over the energy content of the ions.

ACKNOWLEDGMENTS

We would like to thank Andew C. Kummel and Philip J. Brucat for fruitful discussions and donation of Fourier Transform programs. R. N. Zare gratefully acknowledges support through the Shell Distinguished Chairs program, funded by the Shell Companies Foundation, Inc. This work was supported by the Air Force Office of Scientific Research under AFOSR F49620-83-C-0033.

APPENDIX: DATA ANALYSIS

Our method of data analysis can best be understood by first considering the factors that give rise to the metastable peak. An ideal experiment begins with a delta function pulse of ions in space and time. These ions are uniformly accelerated toward the flight tube, with some fraction decomposing per unit time. We measure the ion intensity I as a function of the flight time T. Using elementary physics, we can write the flight time for the ions as a function of the time at which they decompose t_r (see Table I). Inversion of this function allows us to directly obtain I vs t_r, the number of ions decomposing per unit time, from the experimentally measured I vs T. We note, however, in a real experiment the ions are formed during a finite laser pulse and with a distribution of initial velocities and positions. Mathematically, the ideal peak is convoluted with an instrument response function Φ, yielding the experimentally observed peak $I \otimes \Phi$. We merely reverse this process. First a "normal" (undistorted) mass peak is measured. The normal mass peaks result from ions formed at $t_r = 0$, so their shapes are, by definition, the instrument response function. We use the Fourier convolution theorem to perform the deconvolution. Specifically, the deconvolution is carried out by rescaling the normal mass peak to take into account mass dependent resolution[33] and then Fourier transforming this peak and the metastable peak into frequency space. Next, we divide by the instrument peak's Fourier transform. Then, we take the inverse Fourier transform of the result which brings us back to time space. This procedure gives us the I vs T curve corrected for the instrument response function. Mathematically, the procedure cor-

TABLE I. Functional relation between initial conditions and arrival time of daughter ions. The z axis is along the flight path (see Fig. 2).

$$T = t_r + (v_1 - at_r - v_0)/b + ([v_1^2 + 2b(z_2 - z_1)]^{1/2} - v_1)/2 + (z_3 - z_2)/v_2,$$

where

T = flight time,
z_0 = initial position,
v_0 = initial velocity,
t_r = time to reaction in region I,
E_I = field in region I,
E_{II} = field in region II,
M_P = parent ion mass,
M_D = daughter ion mass,
$a = eE_I/M_P$,
$b = eE_I/M_D$,
$c = eE_{II}/M_D$,
z_1 = position of first grid,
z_2 = position of second grid,
z_3 = position of detector,
$v_1 = [(at_r + v_0)^2 + 2b(z_1 - at_r^2/2 - v_0 t_r - z_0)]^{1/2}$; velocity of daughter ion at z_1, i.e., on leaving region I,
$v_2 = [v_1^2 + 2c(z_2 - z_1)]^{1/2}$; velocity of daughter ion at z_2, i.e., on leaving region II.

responds to

$$FT[I(T)] = \frac{FT[I \otimes \Phi]}{FT[\Phi]}, \tag{A1}$$

where

$$I \otimes \Phi = \int_{-\infty}^{\infty} \Phi(t) I(T-t)dt. \tag{A2}$$

Then $I(T)$ is obtained by taking the inverse Fourier transform of Eq. (A1).

Stability of the deconvolution process is obtained by digitally filtering the transformed instrument function, using a modified bandpass filter. The procedure is illustrated in Figs. 11 and 12. Figure 11(a) shows the instrument function and its Fourier transform pair; Fig. 11(b) shows the metastable peak and its Fourier transform pair. Instead of dividing by the transform of the instrument function, we find it more enlightening to multiply by the reciprocal of the transform. This reciprocal is shown in Fig. 12(a) with the physically meaningful region contained within the dotted line box. This box encompasses 95% of the power spectrum of the instrument function; the massive oscillations outside the box correspond to reciprocation of components whose amplitudes are approximately zero. These oscillations are orders of magnitude larger than the signal, and will undesirably amplify high frequency components in the waveform being deconvoluted. The result of the deconvolution, i.e., the inverse Fourier transform of the product of the transform pair from Fig. 11(b) with the transform pair from Fig. 12(a), is shown in Fig. 12(b). Clearly, the noise dominates the signal.

To overcome this problem, we digitally filter the instrument function. We retain unaltered the boxed region in Fig. 12(a), and set the amplitudes of the remaining frequency components equal to a constant. If this constant is zero, we have produced a standard bandpass filter, which cuts off all

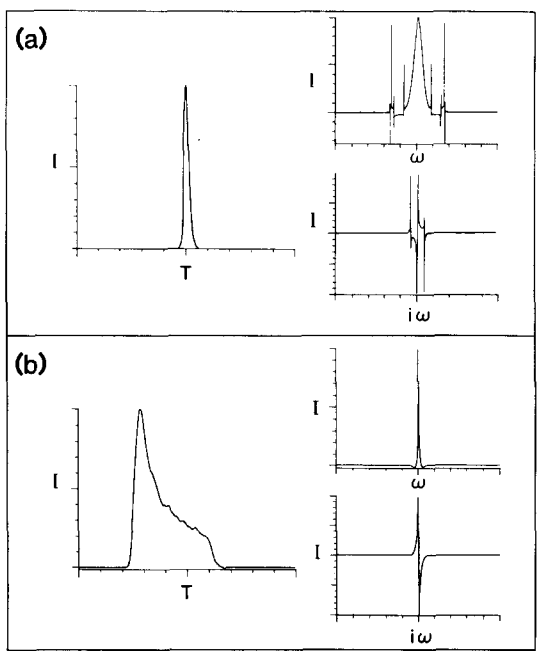

FIG. 11. Waveforms (left) and Fourier transform pairs (right): (a) instrument function and (b) metastable peak.

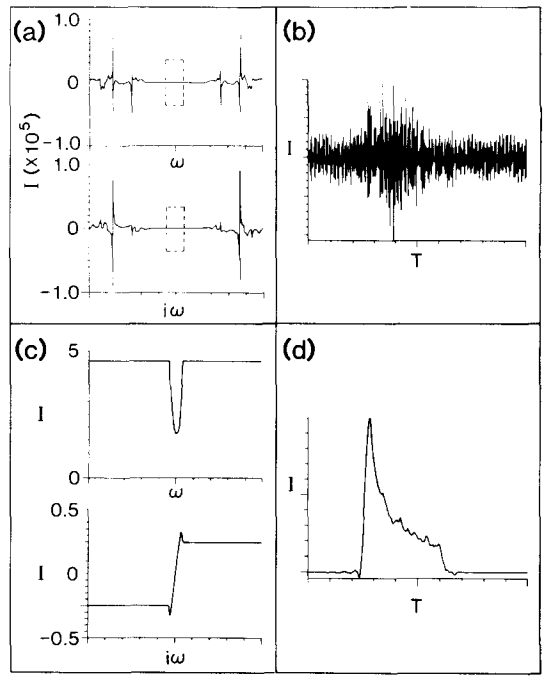

FIG. 12. Data analysis method (see the text): (a) reciprocals of the Fourier transform pair in Fig. 11(a); (b) the resulting deconvoluted waveform resulting from the inverse Fourier transform of the product of the Fourier transform pairs (real and imaginary parts) from Fig. 11(b) and Fig. 12(a); (c) digitally filtered Fourier transform pairs from Fig. 12(a); and (d) the deconvoluted waveform resulting from the inverse Fourier transform of the product of the Fourier transform pairs from Fig. 11(b) and Fig. 12(c).

of the higher frequency components. If this constant is nonzero, as in the present work, it represents the relative amplification of the high frequency components. The result of this filtering is shown in Fig. 12(c) (note change in vertical scale), with the final deconvoluted waveform shown in Fig. 12(d).

The $I(T)$ curve can then be corrected for overlapping isotopic peaks, since these peaks will be shifted to calculable times later than the main peak. We then iteratively solve the equation in Table I for t_r, allowing us to map the $I(T)$ distribution into a distribution of $I(t_r)$.

[1]W. Forst, *Theory of Unimolecular Reactions* (Academic, New York, 1973); T. Baer, in *Chemistry of Ions in the Gas Phase* NATO Advanced Studies Institute, Vimero, Portugal, 1982 (Reidel, Dordrecht, Holland, 1983).
[2]B. Brehm and E. von Puttkamer, Adv. Mass Spectrom. **4**, 591 (1968).
[3]T. Baer, W. B. Peatman, and E. W. Schlag, Chem. Phys. Lett. **4**, 243 (1969).
[4](a) J. H. D. Eland, Int. J. Mass Spectrom. Ion Phys. **8**, 143 (1972); (b) C. J. Danby and J. H. D. Eland, *ibid.* **8**, 153 (1972).
[5]R. Stockbauer, J. Chem. Phys. **58**, 3800 (1973).
[6]A. S. Werner and T. Baer, J. Chem. Phys. **62**, 2900 (1975).
[7]W. Brand and K. Levsen, Int. J. Mass Spectrom. Ion Phys. **35**, 1 (1980).
[8]W. Brand, H. D. Beckey, B. Fassbender, A. Heindrichs, and K. Levsen, Int. J. Mass Spectrom. Ion Phys. **35**, 11 (1980).
[9]W. Brand and K. Levsen, Int. J. Mass Spectrom. Ion Phys. **51**, 135 (1983).
[10]D. Proch, D. M. Rider, and R. N. Zare, Chem. Phys. Lett. **81**, 430 (1981).
[11]T. Baer and T. E. Carney, J. Chem. Phys. **76**, 1304 (1983).
[12]U. Boesl, H. J. Neusser, R. Weinkauf, and E. W. Schlag, J. Phys. Chem. **86**, 4857 (1982).
[13]S. L. Anderson, D. M. Rider, and R. N. Zare, Chem. Phys. Lett. **93**, 11 (1982).
[14]R. N. Compton, J. C. Miller, A. E. Carter, and P. Kruit, Chem. Phys.

Lett. **71**, 87 (1980); J. C. Miller and R. N. Compton, J. Chem. Phys. **75**, 22, 2020 (1981).
[15]J. T. Meek, R. K. Jones, and J. P. Reilly, J. Chem. Phys. **73**, 3503 (1980); J. T. Meek, S. R. Long, and J. P. Reilly, J. Phys. Chem. **86**, 3809 (1982); S. R. Long, J. T. Meek, and J. P. Reilly, J. Chem. Phys. **79**, 3206 (1983).
[16]J. Kimman, P. Kruit, and M. J. Van der Wiel, Chem. Phys. Lett. **88**, 576 (1982).
[17]G. J. Fisanick, A. Gedanken, T. S. Eichelberger IV, N. A. Kuebler, and M. B. Robin, J. Chem. Phys. **75**, 5215 (1981).
[18]Y. Achiba, K. Sato, K. Shobatake, and K. Kimura, J. Chem. Phys. **77**, 2709 (1982).
[19]T. Baer, B. P. Tsai, D. Smith, and P. T. Murray, J. Chem. Phys. **64**, 2460 (1976).
[20]H. M. Rosenstock, R. Stockbauer, and A. C. Parr, J. Chem. Phys. **71**, 3708 (1979); H. M. Rosenstock, R. Stockbauer, and A. C. Parr, *ibid.* **73**, 773 (1980); H. M. Rosenstock (private communication, 1982).
[21]S. T. Pratt and W. A. Chupka, Chem. Phys. **62**, 153 (1981).
[22]G. C. Bjorklund and R. H. Storz, IEEE J. Quantum Electron. **15**, 228 (1979).
[23]Y. S. Jain and H. D. Bist, J. Mol. Spectrosc. **47**, 126 (1973).
[24]S. Rockwood, J. P. Reilly, K. Hohla, and K. L. Kompa, Opt. Commun. **28**, 175 (1979).
[25]U. Boesl, H. J. Neusser, and E. W. Schlag, J. Chem. Phys. **72**, 4327 (1980).
[26]R. B. Bernstein, J. Phys. Chem. **86**, 1178 (1982).
[27]M. A. Duncan, T. G. Dietz, M. G. Liverman, and R. E. Smalley, J. Phys. Chem. **85**, 7 (1981).
[28]D. W. Turner, A. D. Baker, C. Baker, and C. R. Brundle, *Molecular Photoelectron Spectroscopy, A Handbook of He 854* Å *Spectra* (Interscience, New York, 1970).
[29]M. Allen, J. P. Maier, and O. Marthaler, Chem. Phys. **26**, 131 (1972); J. P. Maier and O. Marthaler, *ibid.* **32**, 419 (1978); J. P. Maier, in *Kinetics of Ion–Molecule Reactions*, edited by Pierre Ausloos (Plenum, New York, 1979).
[30]R. C. Dunbar, H. H. Teng, and E. W. Fu, J. Am. Chem. Soc. **101**, 6506 (1979).
[31]H. M. Rosenstock, K. Draxl, B. W. Steiner, and J. T. Herron, J. Phys. Chem. Ref. Data **6**, Suppl. 1 (1977).
[32]T. Baer and R. Kury, Chem. Phys. Lett. **92**, 659 (1982).
[33]The amount by which the instrument peak was rescaled was estimated from Monte Carlo results for peak width as a function of mass. For rescaling the mass 112 peak to the mass 77 peak, we use a factor of 0.617.